Paradigmatic case of long-term colocated wind–wave energy index trend in Canary Islands

Alain Ulazia [a],*, Jon Sáenz [b,d], Aitor Saenz-Aguirre [a], Gabriel Ibarra-Berastegui [c,d], Sheila Carreno-Madinabeitia [e]

[a] Energy Engineering Department, University of the Basque Country (UPV/EHU), Engineering School of Gipuzkoa-Eibar, Spain
[b] Department of Physics, University of the Basque Country (UPV/EHU), Sarriena Auzoa z/g, 48940 Leioa, Spain
[c] Energy Engineering Department, University of the Basque Country (UPV/EHU), Alda, Urkijo, 48013 Bilbao, Spain
[d] Plentziako Itsas Estazioa, PIE (BEGIK), University of the Basque Country (UPV/EHU), Areatza Pasealekua, 48620 Plentzia, Spain
[e] Department of Mathematics, University of the Basque Country (UPV/EHU), Paseo de la Universidad, 01006 Vitoria-Gasteiz, Spain

ARTICLE INFO

ABSTRACT

Previous studies based on remote sensing data and reanalysis have identified strong historical increments of wind speed in the area around the Canary Islands (Spain) without appreciating any increment of wave height. This decoupling of long-term trends for wind and wave data is not very common, and can be considered paradigmatic for an innovative study, with important implications for wind and wave hybrid or co-located energy production. In this study, wind and wave data from ERA5 reanalysis in the area around the Canary Islands have been used to compute a wind–wave energy co-location feasibility index between 1981–2020 showing an increment of the index above +5%/decade. Furthermore, realistic wind and wave energy production has been calculated at an interesting hot-spot using a specific floating wind turbine co-located aside a oscillating buoy type wave energy converter. The corresponding capacity factor trend for wind energy (+0.8%/decade) and capture width ratio evolution for wave energy (−1.5%/decade) shows also the wind–wave decoupling, which constitutes a significant result for an original approach.

1. Introduction

Renewable energy is showing a significant increase, almost doubling the share of energy from renewable sources in gross final energy consumption in the case of Europe [1]. However, 80% of current energy supply is still delivered by fossil fuels [2], and each country must include a decarbonization policy based on renewable energy sources to obtain a carbon-neutral society through further development of clean technologies and sustainable multi-period selection of locations [3]. For instance, Iberian Peninsula and Canary Islands constitute a paradigmatic case due to the their high wind and solar energy potential, showing very good previsions for their techno-economic assessment [4]. This will certainly contribute to meet the Spanish CO_2-reduction objectives. This is an important issue since by 2030 Spain is committed to generate more than 74% of its electricity from renewable sources [5].

Among renewable energy sources, Ocean Renewable Energy (ORE) can offer a huge potential for electricity generation, mainly using the combination of wind and wave energy, as it was shown in specific geographical areas such as the Mediterranean [6] or the Chinese Sea [7], or within sustainable development objectives using renewable energy strategies in Europe [8].

In general terms, currently wave energy exhibits rather low Technology Readiness Level (TRL) values [9] and is not so technically developed as offshore wind technology. However, recent innovations have shown the potential of wave farms near the coast at providing a continuous apportion of energy into the grid [10]. In the case of a particular technology – Oscillating Water Column (OWC) – the TRL is currently at a value of 8 [11].

Recent studies on a fully operational wave farm [12], indicate that the energy generated by waves are predictable to a high extent in the short term, thus allowing the development of electricity management protocols to be applied in the overall energy market. An important challenge is the determination of how climate-driven changes in wave energy, will impact on the future electricity generated at a wave farm designed under current-day conditions. Similarly, future changes of

List of Abbreviations

C3S	Copernicus Climate Change Service
ECMWF	European Centre for Medium-Range Weather Forecasts
ERA5	5th reanalysis by ECMWF
ERA-Interim	4th reanalysis by ECMWF
FB	Floating Body wave energy converter
IFS	Integrated Forecasting System
LCOE	Levelized Cost of Energy
NCAR	National Center for Atmospheric Research
NCEP	National Centers for Environmental Prediction
NREL	National Renewable Energy Laboratory
ORE	Ocean Renewable Energy
OWC	Oscillating Water Column
TRL	Technology Readiness Level
WEC	Wave Energy Converter
WT	Wind Turbine

Nomenclature

AEP	Annual Energy Production (kWh)
B	Frontal absorption width and diameter of the WEC
$c(0)$	Instantaneous Correlation
CLF	Colocation Feasibility Index
CF	Capacity Factor
CI	Confidence Interval
CWR	Capture Width Ratio (m)
D_b	Diameter of the floating body
g	Acceleration of gravity (9.8 m/s^2)
H_s	Significant wave height (m)
M	Molecular mass of dry air (28.9 kg/kmol)
N	Number of hours per year (8760 h)
p	Pressure (Pa)
$P(U_i)$	Wind turbine power for wind speed U_i (kW)
P_{abs}	Absorbed Power of the WEC (kW)
P_{wave}	Theoretical Power of the wave front (kW)
P_R	Rated power of the wind turbine (kW)
R	Constant of ideal gases
t	Temperature (K)
T_m	Mean wave period (s)
T_e	Energy period of waves (s)
U	Wind speed (m/s)
U_x	Wind speed at x m height (m/s)
WEF	Wave Energy Flux (kW/m)
WPD	Wind Power Density (W/m^2)
z_0	Sea roughness (m)
$\alpha_{i,j}$	CLF index weight coefficients
ρ	Real air density (kg/m^3)
ρ_0	Standard air density (kg/m^3)
ρ_w	sea water density (kg/m^3)
σ	Standard deviation
ΔT	Time resolution (1 h)

lent robustness and adaptability to wave climate changes [13]. Coming to the impact of sea-level rise on wave farms a recent study [14] suggests that it may be negligible. Therefore, predictability in the short term and robustness before long-term changes seem to be two major characteristics of wave energy.

The combined exploitation of wind and wave energy is therefore drawing increasing attention in the recent scientific literature, showing strong synergies not only for energy production, but also for operation, maintenance, and protection of floating wind turbines and its structures against extreme events [15]. Although ocean extreme event analysis is an important aspect, it falls out of the scope of this study. Extreme event related index establishes a cut-off for the installation of offshore structures due to security issues. It is therefore a discrete indicator instead of a continuous one like a feasibility index related to the optimal combination of wind–wave. It is supposed that before a wind–wave feasibility study, or any other kind of wind and wave energy potential study, an extreme event assessment should verify whether an offshore installation is both, technologically and economically viable or not. Beyond these security and survival problems, this study is related to the optimal combination and hybridization of wind energy and wave energy.

This combined approach [16] can play a key role at meeting the European objective for hydrogen production [17]. The present study emphasizes the importance of long-term wind [18] and wave energy trend analysis developed by the authors for Mutriku wave plant [13], Gulf of Biscay [19], Ireland [20] or Iceland [21], now, in a completely different environment. Now, instead of carrying out two independent analyses for wind and waves, this work constitutes a novel approach for the estimation of historical trends for the combined resource. To that purpose, a paradigmatic oceanic area such as the Canary Islands has been selected for this study, where the predominant wind (trade winds) and the swell (from the Atlantic Ocean) are aligned in opposite directions.

All the seven islands of the Canary Archipelago show a great potential in OREs. El Hierro is referential in this sense, being a relevant case around the world for a totally independent electrical energy system based on wind energy with the wind-hydro project Gorona del Viento [22], and also with a high wave energy potential [23]. Other islands such as Tenerife and Gran Canaria also exhibit an important offshore wind and wave energy potential [24,25], and it can be concluded that this hybrid potential is generally strong for the seven islands.

The study of historical wave energy and wind energy trends at the global scale have commonly shown a combined increment of both resources in the last decades, which has been hypothetically related to the effects of climatic change. This synchronized increment of both resources is well known based on reanalysis data or remote sensing data. Young et al. [26] used satellite data since the 80 s to the 90 s to compute global trends of wind speed and wave height, and this synchronized increment is general in the Atlantic Ocean with the exception of Macaronesian area and the Guinean Gulf. In other Atlantic regions like the Bay of Biscay in the last decades, the observations indicate a combination of positive trends for wave energy and a not clear pattern for wind speed [13]. All this makes Canary Islands an area of scientific interest for this type of studies. The special character of the Canarian marine climate within the interaction of wind and waves is also shown by the influence of trade winds on trans-hemispheric swell waves [27], or by singular ocean currents derived from a strong continental slope [28].

This fact makes the Canary Islands a paradigmatic case to study the historical evolution of wind and wave energy combination, which in this work, will be studied using reanalysis data and decadal trends of both resources. The focus will be to use a fine resolution analysis at previously identified hot spots based on a wind–wave co-location index [29] and the consequent optimal strategies of deployment of co-located wind–wave energy farms [16]. The discussion on the adoption of an analytical or a subjective index to measure the feasibility of the

sea level could also have an impact on the future electricity output some decades from now. Although uncertainties remain about these two issues, at least Oscillating Water Column (OWC) type converters – mainly due to their regulation mechanisms – seem to exhibit an excel-

Table 1

Comparison between the properties of ERA5 and the previous ECMWF's reanalysis ERA-Interim.

Properties	ERA-Interim	ERA5
Availability	1979 onwards	1950 onwards
IFS model cycle	31r2 (2006)	41r2 (2016)
Data assimilation	12-hour 4D-Var	12-hour 4D-Var ensemble
Spatial resolution	79 km (TL255) 60 levels to 10 Pa	31 km (TL639) 137 levels to 1 Pa
Ocean waves	1 degree	0.5 degree
Output frequency	6-hourly for analyses 3-hourly for forecasts	Hourly throughout (uncertainty 3-hourly)
Output parameters	Extensive	Extended (e.g. 100 m wind)

hybridization of both OREs is beyond this article due to its mathematical nature, but it opens a rich research line in analogy to other kind of indexes to measure techno-economic aspects such as energy poverty, as it is described in Section 4 [30].

The reminder of the paper is structured as follows: after the introduction on the state of art of the hybridization of wave energy and wind energy, the specific ERA5 data used for this study will be explained (Section 2.1); then the methodology on the computation of decadal evolution in Section 2.2.2, and the description about the co-location feasibility index (CLF) in Section 2.2.3 will be shown. A specific section will be devoted to the method of computation on real energy production based on the power curve of specific turbine (Section 2.4.1) along with the power model of a specific wave energy device (Section 2.4.2); Section 3 shows the decadal resource maps, the evolution of co-location index, and the evolution of real wave and wind energy production. The Discussion Section 4 interprets qualitatively these results, and finally, Section 5 concludes with a fundamental summary and outlooks for future developments.

2. Data and methods

The following sections describes the data sources used for the study and the corresponding methods to develop the results.

2.1. Data

The following sections describe the ERA5 reanalysis and the study area around Canary Islands, where the data sources are implemented.

2.1.1. ERA5 reanalysis

Long-term variations of the wave and wind resource have been analysed employing ERA5 reanalysis data [31]. The European Centre for Medium-Range Weather Forecasts (ECMWF) processes all datasets using their Earth System model Integrated Forecasting System (IFS) and the results are distributed by the Copernicus Climate Change Service (C3S) and it already covers the period from 1950 to present [32]. This reanalysis combines huge amounts of historical observations from satellites, in-situ met-ocean data (onshore meteorological stations and offshore buoys), and snow data.

The ERA5 reanalysis is the fifth major global reanalysis produced by the ECMWF (after ERA-Interim, see Table 1), and provides 1-hourly data at a spatial resolution of around 30 km all over the world for downloaded meteorological data:

1. For atmosphere and wind energy analysis these parameters are used: wind speed (U), pressure (p), and temperature (t).
2. However, in the case of wave data, the spatial resolution available is about 50 km, where these parameters are used: significant wave height (H_s) and mean wave period (T_m) or peak wave period (T_p).

Recent literature describes good evaluations of ERA5 against wind and wave observations, and not only for low roughness and turbulence areas of the ocean, but also for less predictable onshore locations in case of wind farms:

- Versus wind farm data in the North of Europe [33];

- In the Iberian Peninsula versus offshore buoys anemometers [18];
- For Iberian and Canarian buoy wave data [34];
- For swell wave data [35];
- For global wave data versus altimeter measurements [36] ;
- In China waters for wave data [37].

2.1.2. Study area

The climate of the Canary Island has long ago been identified as very interesting for wind energy due to the fact that the islands are located, especially during summer, under a strong influence of North-Easterly trade winds associated to the Azores high pressure system. These summer trade winds are very regular and very frequently blow with speeds between 7 m/s and 11 m/s [38]. The Azores high represents during summer the surface response of the pressure field to the subsidence associated to the Hadley Circulation in the Atlantic sector, and some studies show that there is a positive trend in the area-averaged pressure of the Azores High [39], which makes the area interesting for a study like this one, which addresses the long-term behaviour of energy resources of the area. Furthermore, given its political membership to the European Union (Spain) in contrast to its geographical African origin in the form of volcanic islands, it constitutes a very interesting area for a isolated electrical grid based on renewable energies with few interconnections [40].

One-hourly data from 1981 to 2020 (40 years) have been downloaded in the Canary Islands for the present study, meaning that 350640 cases are analysed at each gridpoint in the analysed area, which covers longitudes in the interval [−19°E, −13°W] and latitudes in [27°N, 30°N], which is composed of 91 gridpoints in total for the geographical window that covers the seven Canary Islands: El Hierro, La Palma, La Gomera, Tenerife, Gran Canaria, Lanzarote and Fuerteventura.

The steep bathymetry around the islands due to its volcanic origin is shown using shaded areas in Fig. 1, which reaches up to −5000 m depth in few kilometers [41]. In Section 3.2, a point of interest is selected for the behaviour of CLF at the South of Tenerife, where a zonal bathymetry transect (under the map) and meridional transect (on the left) are plotted as white lines through the point −17°E and 27.5°N. Both show that the sea deepens to thousands of meters in few kilometers from the coast and that the hot-spot depth is around −3500 m.

2.2. Methods

The following sections derive the main parameters that interpret the results from the basic parameters of ERA5, describe the method of computation of these parameters' trend per decade, and defines the CLF that determines the performance of wind–wave combination at a given location.

2.2.1. Derived magnitudes

The Wave Energy Flux (WEF) is the usual indicator to characterize the energy transported by waves. It is stated in [kW/m], and is derived from the H_s and energy (mean) wave period (T_e) [42,43] according to Eq. (1).

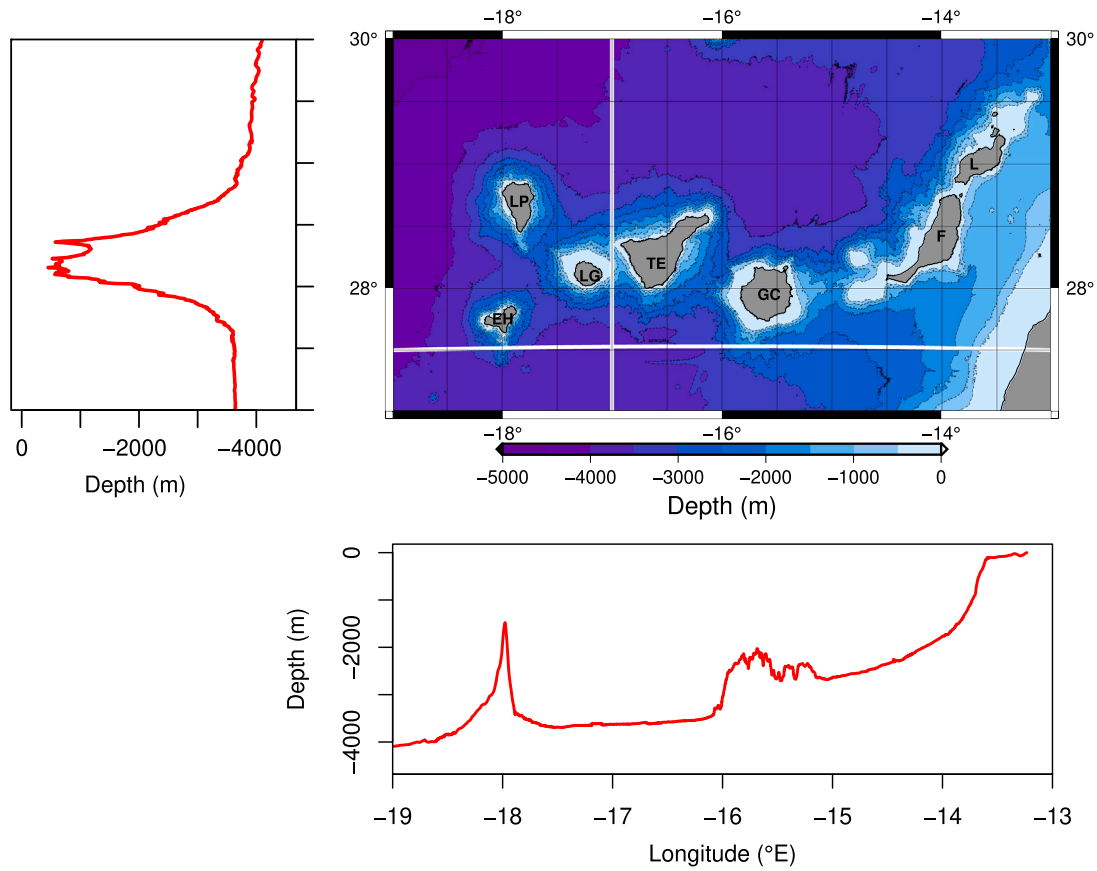$$WEF = \frac{\rho_w g^2}{64\pi} H_s^2 T_e = 0.49 H_s^2 T_e \tag{1}$$

Fig. 1. Map of the Canary Islands, with black labels showing the main islands (EH: El Hierro, LP: La Palma, LG: La Gomera, TE: Tenerife, GC: Gran Canaria, F: Fuerteventura and L: Lanzarote). The bathymetry around the islands is shown using shaded areas and the location of the buoys used in the study are shown by stars and labelled in red (TS: Tenerife Sur, SCT: Santa Cruz de Tenerife, GC: Gran Canaria, LPE: La Palma East). One meridional (zonal) transect through the point $-17°$E and $27.5°$N is shown to the left (under) the map for reference and as white lines drawn in the map.

It is to be taken into account that ERA5 denominates mean wave period to the energy period T_e [44] so the calculation of WEF is straightforward using (1) under the assumption of deep waters conditions. In the case of Canary Islands, this condition is met given its deep bathymetry as shown in Fig. 1.

On the other hand, the magnitude that defines the kinetic power of the wind is the Wind Power Density (WPD), and is given by Eq. (2):

$$WPD = \frac{1}{2}\rho U^3 \tag{2}$$

where ρ is the air density, calculated every hour from p and t, together with the molecular mass of the air $M=28.9$ kg/kmol, and the constant of the ideal gases $R=8314$ KJ/kgK.

$$\rho = \frac{pM}{Rt} \tag{3}$$

After developing specific tools to reduce the huge computational effort involved [45,46], it is to be highlighted that the authors have shown in many previous studies the impact of air density changes in wind energy production. Instead of considering the standard value of 1.225 kg/m^3 as a constant in wind energy studies, authors have shown the impact of seasonal ρ variations as well as the small influence of humidity changes in the WPD at a given height and location annually [47] and seasonally [48].

2.2.2. Decadal evolution

The decadal evolution of WEF and WPD density has been computed in percentage terms in both cases, by comparing the differences of the decadal averages of WEF (i.e., last decade WEF_4 for 2011–2020 minus first decade WEF_1 for 1981–1990) with respect to the first

decade:

$$100\frac{WEF_4 - WEF_1}{WEF_1} \tag{4}$$

The same can be done for the 3rth and 2nd decades, and for the WPD trend (see Fig. 3).

2.2.3. Colocation index for wind and waves

The CLF for wind and wave energy defined by Astariz et al. is used in this study [29]. It depends on WEF and WPD, and on the instantaneous correlation ($c(0)$) or the standard deviation of both magnitudes (σ_{WEF} and σ_{WPD}). For the sake of brevity in this archival paper, the equation is not defined, but the general interpretation is simple, since it constitutes a score between 0 and 1, with 1 at the maximum co-location feasibility for the combination of wind and wave energy. According to Eq. (5), there are statistically weighted five terms in the equation for a given study area ranged between 0 and 1.

$$
\begin{aligned}
CLF_i = &\ \alpha_{WEF}\frac{WEF_i - WEF_{\min}}{WEF_{\max} - WEF_{\min}} \ (1)+ \\
&\ \alpha_{WPD}\frac{WPD_i - WPD_{\min}}{WPD_{\max} - WPD_{\min}} \ (2)+ \\
&\ \alpha_{c(0)}\frac{c(0)_{\max} - c(0)_i}{c(0)_{\max} - c(0)_{\min}} \ (3)+ \\
&\ \alpha_{\sigma_{WEF}}\frac{\sigma_{WEF,\max} - \sigma_{WEF,i}}{\sigma_{WEF,\max} - \sigma_{WEF,\min}} \ (4)+ \\
&\ \alpha_{\sigma_{WPD}}\frac{\sigma_{WPD,\max} - \sigma_{WPD,i}}{\sigma_{WPD,\max} - \sigma_{WPD,\min}}
\end{aligned}
\tag{5}
$$

Table 2
Main characteristics of the baseline NREL 5 MW wind turbine.

	Value	Unit
Rated power	5	MW
Rotor diameter	123	m
Hub height, diameter	90, 3	m
Cut-in, rated, cut-out wind speed	3, 11.4, 25	m/s
Cut-in, rated rotor speed	6.9, 12.1	rpm

1. The ratio between the difference of mean WEF with respect to the minimum WEF of the region and the difference between the maximum and minimum WEF.
2. The ratio between the difference of mean WPD with respect to the minimum WPD of the region and the difference between the maximum and minimum WPD.
3. The temporal correlation of WPD and WEF at each gridpoint.
4. The ratio between the difference of the standard deviation of WEF with respect to the maximum standard deviation of the region and the difference between the maximum and minimum standard deviations.
5. The ratio between the difference of the standard deviation of WPD with respect to the maximum standard deviation of the region and the difference between the maximum and minimum standard deviations.

Obviously, the five terms should be between [0,1], and being i substituted by WEF, WPD, $c(0)$, σ_{WEF}, or σ_{WPD},

$$\sum_i \alpha_i = 1 \tag{6}$$

In this way, according to the points 1 and 2 the average value of WPD and WEF at the location should be as high as possible (near the maximum of the region) to improve CLF. The same can be said for the correlation between WPD and WEF. However, the points 4 and 5 establish that the standard deviations of σ_{WEF} and σ_{WPD} should be as low as possible (low variability near the minimum of the region) in order to raise the value of CLF.

2.3. Annual trends at a selected location

The previous spatial method will be used to select a hotspot and interesting location due to WPD and WEF variations. After this selection, a finer methodology is used at this location to find the annual variations of co-location feasibility and real energy production.

The computation of the annual trends of CLF and real productions using Capacity Factor (CF) and Capture Width Ratio (CWR) (see Sections 2.4.1 and 2.4.2) will be represented by linear regression and Theil–Sen method [49], which is a robust estimator which reduces the sensitivity of the trend to outliers by considering the medians instead of geometrical averages.

2.4. Real energy production

The theoretical methods developed previously will be further developed introducing wind and wave data in power curves and power matrices of real wind turbines and Wave Energy Converters (WECs). This final approach can therefore offer strong commercial interpretations in the results.

2.4.1. Wind turbine
The wind data at the identified hot-spot have been implemented on the power curve of the National Renewable Energy Laboratory (NREL) 5 MW wind turbine [50] for the computation of the Annual Energy Production (AEP) and the CF. Table 2 describes the main characteristics of the turbine.

However, previously, the wind speed at 10 m has to be raised to the wind speed at the hub height (90 m) by the log law [51]. The instantaneous one-hourly roughness (z_0) of the sea is obtained from wind speed at 10 m (U_{10}) and at 100 m (U_{100}) by Eq. (7).

$$\frac{U_{100}}{U_{10}} = \frac{\log(100/z_0)}{\log(10/z_0)} \Rightarrow z_0 = e^{\frac{\log(10)(2U_{10}-U_{100})}{U_{10}-U_{100}}} \tag{7}$$

After that, wind speed at the hub height is obtained using the log law in Eq. (8).

$$U_{90} = U_{10} \frac{\log(90/z_0)}{\log(10/z_0)} \tag{8}$$

Furthermore, the normalization of the wind speed is given by the cubic root of the ratio between air densities, being ρ_0 the standard air density, and ρ the real air density [48] (see Eq. (9)).

$$U_{90n} = \left(\frac{\rho}{\rho_0}\right)^{\frac{1}{3}} U_{90} \tag{9}$$

Finally, the annual production AEP (kWh) is given by Eq. (10), where N=8760 is the hours per year, $P(U_i)$ is the power produced in kW by the turbine for each wind-speed U_i of the time series, and $\Delta T = 1h$, the time resolution of the time series.

$$AEP = \sum_{i=1}^{N} P(U_i)\Delta T \tag{10}$$

AEP is divided by the ideal production at rated power $P_R = 5000$ kW to obtain CF according to the Equation

$$CF = \frac{AEP}{P_R \cdot 365.25 \cdot 24} \tag{11}$$

This parameter CF is selected as an adimensional ratio in order to normalize the real production of the wind turbine and compare it with other ratio (CWR) that expresses an similar concept of the selected WEC, see Section 2.4.2.

2.4.2. Point absorber wave energy converter
A WEC model of floating body type of developed by Oigarden and Olsen was used in deep water condition [52,53], having the absorbed wave power P_{abs} in kW as a function of H_s and T_p :

$$P_{abs} = 4.5 D_b^{2.4} H_s^{1.7} T_p^{-0.9} \tag{12}$$

. where D_b denotes the diameter of the floating body. $D_b = 2$ m is adopted in the first approximation by the inventors [52], and in the 40 years evolution presented in Section 3.3.3.

This WEC was designed to be partially filled with water, changing the water volume within, thus adapting the natural frequency of the device to the incident wave period.

Therefore, CWR can be obtained considering P_{abs} as the really absorbed power, and P_{wave} the theoretical wave power given by WEF along the transversal longitude of the wave for D_b (frontal width of the device $B = D_b$).

$$CWR = \frac{P_{abs}}{P_{wave}} = \frac{P_{abs}}{WEF \cdot B} \tag{13}$$

This parameter, CWR, is selected as an adimensional ratio in order to normalize the real production of the WEC device and compare it with wind turbine's CF, which is also a ratio.

3. Results

The Table 3 summarizes all the main results and the confidence intervals at 95% confidence level for CLF, CF, CWR, and the real power production of the wind turbine and the WEC. In the next sections, the origin and visual representations of these final values are shown with a brief interpretation of these previous results.
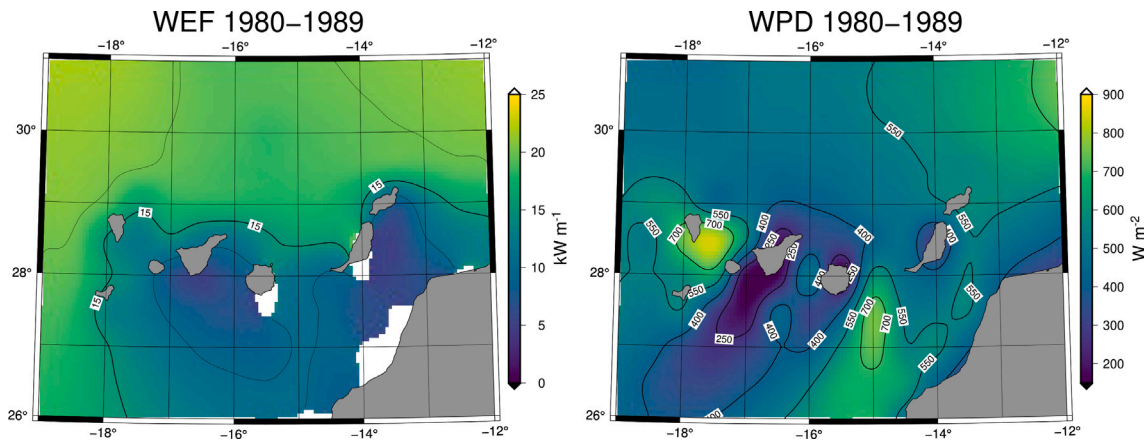
Fig. 2. Absolute average value in the 1980–1989 initial decade of WEF (left in kW/m) and WPD (right in W/m²).

3.1. Resource maps of decadal differences

Fig. 2 shows the average WEF (left) and WPD (right) from 1980 to 1989, the first referential decade with respect to which the relative variations of the following decades will be computed. For the following interpretation of the final results it should be noted the strong reduction of wind energy potential in the Southwest of Tenerife (around 200 W/m² at 10 m height), under the protection of Northeastern trade winds (around 500 W/m² in the North with peaks of 900 W/m² between islands), an effect that is also considerable for WEF, but in a weaker way (from 15 kW/m to 10 kW/m). These spatial distributions are very similar to values found in previous literature for wave energy assessment and offshore wind energy assessment [25,54].

The decadal differences in percent for WEF and WPD (Fig. 3) show a relevant increase, which reach up to 15% and 18% between the main islands of Tenerife and Gran Canaria for the last decade during the 2010s. In the case of WPD, there is even a decrease near the coast of Africa that reaches -5%, but the general trend is clearly incremental during the decades.

However, the increment difference between WEF and WPD (Fig. 4) is the relevant question here, in order to analyse the decadal variation of the feasibility of wind and wave energy combination. This study shows a huge difference of 18% between both historical trends at a gridpoint in the south of Tenerife and La Palma (longitude = $-17°$E, latitude = 27.5°N), due to the high increase of WEF and the reduction of WPD from the decade of 1980s to the last decade of 2010s. This location also corresponds to the highly protected area from trade winds according to energy potential maps of Fig. 2.

3.2. Evolution of the co-location index at a relevant location

The identified hotspot at the mentioned gridpoint ($-17°$E, 27.5°N) will be used for the study of the annual evolution of CLF during the 40 years of analysis. Thus, the five terms of the CLF equation have been computed for each year from 1980 to 2019 with around 350400 cases analysed, and statistical weight of each term has been subjective keeping the values of the original work of Astariz et al. [29], and weighting above all the index for the values of wave energy and wind energy, lower for the correlation, and giving a low specific weight to the variability for the two standard deviations (see Expression (14)).

$$\alpha_{WEF} = 0.35; \ \alpha_{WPD} = 0.35; \ \alpha_{c(0)} = 0.2; \ \alpha_{\sigma_{WEF}} = 0.05; \ \alpha_{\sigma_{WPD}} = 0.05;$$
$$(14)$$

This election according to [29], establishes the same index weight for WEF and WPD, not only for their absolute values (α_{WEF} and α_{WPD}), but also for their variability within the standard deviation of the signals ($\alpha_{\sigma_{WEF}}$ and $\alpha_{\sigma_{WPD}}$).

Fig. 5 shows a clear increment of CLF along the 40 years from 0.44 to 0.51, showing also the confidence interval of the trend at a 95% confidence level using Theil–Sen method [49]. Although the value of WPD remains almost constant at this point, this positive evolution is due to the strong increment of WEF at this point, which has a high statistical weight (0.35). The low variations of the correlation and standard deviations does not affect the final product of CLF.

3.3. Real energy production

The evaluation of the annual real production considering the power curve of the NREL 5 MW wind turbine for the computation of CF (see Section 2.4.1), and the floating device model's annual average CWR (see Section 2.4.2), show approximately a similar behaviour: positive in the case of the wind turbine (Fig. 7), and negative in the case of the WEC (Fig. 8). The selected gridpoint using the described CLF method shows therefore a long-term wind–wave energy compensation also for realistic electrical energy production. For that, previous to the energy production estimations, the first following Section 3.3.1 analyzes the instantaneous wind and wave power in kW considering the entire time series of four decades 1-hourly.

3.3.1. Power production by decades

Firstly, Fig. 6 shows the decade boxplots of each device, the floating body (a) and the wind turbine (b), according to their instantaneous production in kW at each moment of the time series (40 years, 1 hourly). Although there is a relevant increment of power production for waves, it is no clear the trend of wind power production. This instantaneous power will be the base for the computation of CF and CWR in the following sections.

3.3.2. Evolution of the annual capacity factor of the wind turbine

The selected gridpoint does not show a good CF, since the best offshore locations' CF reach 0.40–0.50, but it is above a reasonable limit approximating 0.30 [55]. However, the 40-year trend is positive, showing a relevant increment at a 95% confidence level described by the shaded area (See Table 3). The linear fitting method or the Theil–Sen method [49] show a similar slope value and confidence interval, with a rise of CF around 0.02 starting from 0.27 in 40 year period. Table 3 in Section 4 shows the exact values of the confidence interval.

3.3.3. Evolution of the annual average capture width ratio of the floating device

The selected gridpoint shows a reasonable CWR for a floating device around 0.40–0.50 [56]. The 40-year trend is again relevant at a 95% confidence level, but there is a reduction of the value (See Table 3). The negative slope computed by the linear method or the Theil–Sen method [49] are similar, showing an absolute reduction of CWR around 0.02 starting from 0.45.
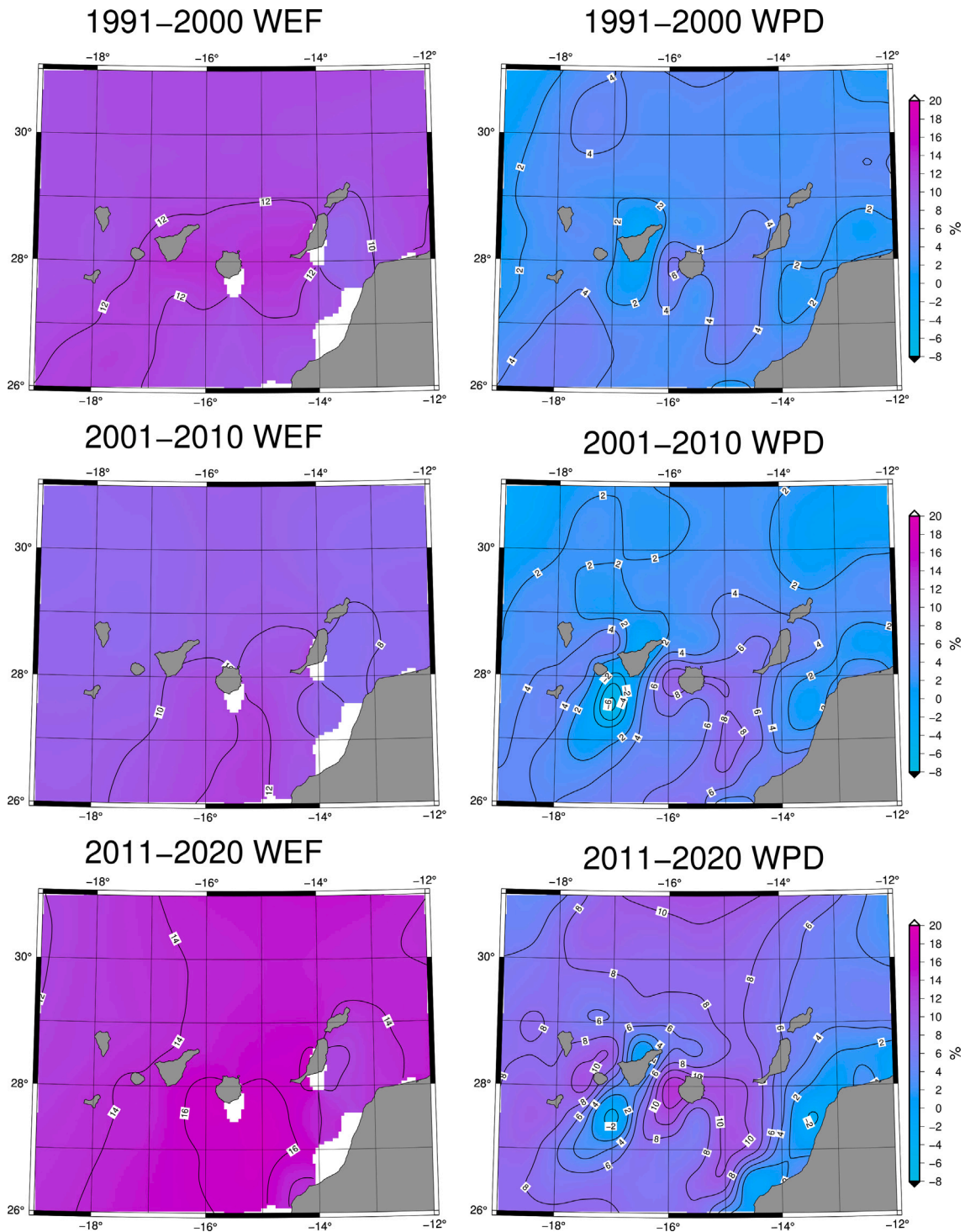
Fig. 3. Decadal differences with respect to 1980s initial decade in percent (by rows) for WPD (left column) and WEF (right column).

4. Discussion

A statistical summarizing of the previous graphical results shows the significance of the obtained confidence intervals and trends. Table 3 resumes the confidence intervals (CI 95%) calculated by means of the Theil–Sen method for the trend analysis of CLF, CF and CWR per decade (by columns). Wind turbine's (WT) and floating body's (FB) power (kW) is also shown in the final rows. The last column shows the slope in percent per decade according to the central value.

Although the positive trend of WT's CF is not statistically significant, the numeric values of the inverse trends of wave energy and wind energy are coherent with the previous graphical representations, and the final result in percent per decade show very relevant variations mainly for the negative slope of CWR and the positive value of CLF that reaches the 5%. This is a very important value, since a projection of this trend along a century would increment the co-location index from 0.4–0.5 to 0.7–0.8. It should be noted also the strong increment in percent of FB's power due to the increment of WEF, which is offset in the calculation of CWR due to the increase of the divisor in Eq. (13).

These strong trends are not strange, because previous literature on global historical trends of wind speed and wave height shows a
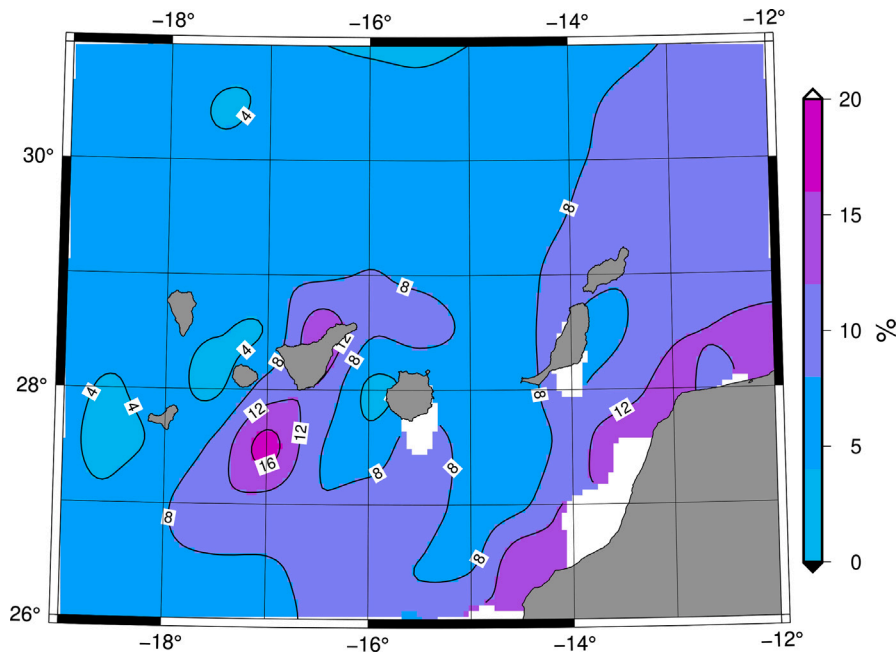
Fig. 4. Increment difference in four decades (2011–2010 minus 1980–1989) between WEF and WPD.
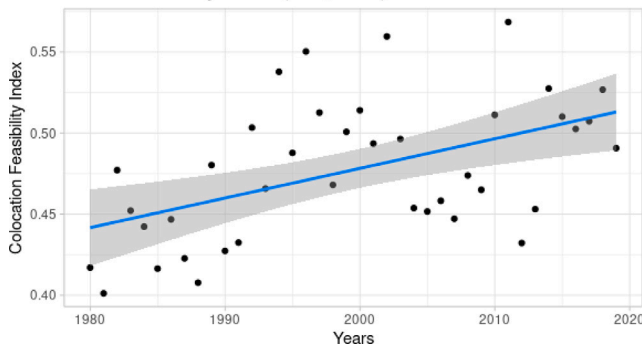

Fig. 5. CLF trend at the identified hotspot.

Table 3

This table summarizes the main results of this article, showing the numerical values of the trends per decade with their confidence intervals. In columns, confidence intervals (CI 95%) of the Theil–Sen method for the inferior, central and superior value (per decade). In rows, the Co-location Feasibility index, Capacity Factor, capture width ratio, and the Wind turbine and floating body power in kW. The last column shows the decadal increment in percent based on the central value.

CI 95%	Inferior	Central	Superior	%/10y
CLF	0.01	0.020	0.025	+5.6
CF	0.000	0.0017	0.0040	+0.8
CWR	−0.010	−0.007	−0.005	−1.5
WT (kW)	−2.3	21.7	26.6	+1.6
FB (kW)	0.13	0.16	0.27	+17

synchronized general increment in the Atlantic Ocean with the exception of the North-West African coast, Guinea Gulf, and Canary Islands [26,57]. This fact has been also corroborated by this study showing not only the decoupling of WEF and WPD, but also the corresponding decoupling of wind energy and wave energy production by a selected wind turbine and WEC according to CF and CWR (see Figs. 7 and 8).

High resolution Global Wind Atlas [58] also validates the CF values identified at the hot-spot ($-17°$E, 27.5°N), under the protection of trade winds, with values around 0.30. This global atlas offers wind resource mapping at 250 m horizontal grid spacing, and CF resource mapping at 10, 50, 100, 150 and 200 m above ground/sea level. Since the extension of the ERA5 grid reaches the 0.5° resolution, the Global Wind Atlas shows that these data correspond to the area at the South of La Gomera, where CF reduces significantly near the coast even below 0.20.

The adoption of subjective specific weighs for the α parameters in Expression (14) and Eq. (5) can be improved in the future using analytic mathematical methodology for index generation, as it is used in other kind of energy index generation such in the case of energy poverty in a multidimensional approach [59]. The incorporation of analytical criteria to axiomatically determine the α parameters can be very interesting in future research, introducing, for instance, Levelized Cost of Energy (LCOE) values of offshore wind energy and wave energy to select a ratio between α_{WEF} and α_{WPD}. This fact would be important in the construction of a new analytical index given the lower LCOE of offshore wind energy up to 160 €/MWh [60] compared to wave energy's LCOE, which is between 370–1200 €/MWh [61].

According to these preliminary data, α_{WPD} and α_{WEF} can be different in a future research that would modify the original adoption of Astariz et al. [62], but this approach would therefore constitute a new and deeper axiomatic in analytical hierarchy process described by mathematicians in applications to index generation [63]. Anyway, this new approach would need to open a future research line between mathematics and techno-economic wave energy engineering, introducing also the statistics about survivability risk and extreme oceanic events as a previous step of the mathematical modelling of the improved index.

It is not possible currently to attribute the detected trends to climate change induced by increased concentration of greenhouse gases. Local analyses located north of the Canary Islands using National Centers for Environmental Prediction/National Center for Atmospheric Research (NCEP/NCAR) data show that Northern Hemisphere models of variability such as the North Atlantic Oscillation or decadal signals in the ocean such as the Atlantic Multicedal Oscillation [64] affect the area. On the other hand, even though some papers identify a widening (poleward shift) of the Hadley Cell during the last decades [65], there are still some doubts regarding the seasonal or regional characteristics of the expansion of the tropics [66]. Besides that, the relevant literature has
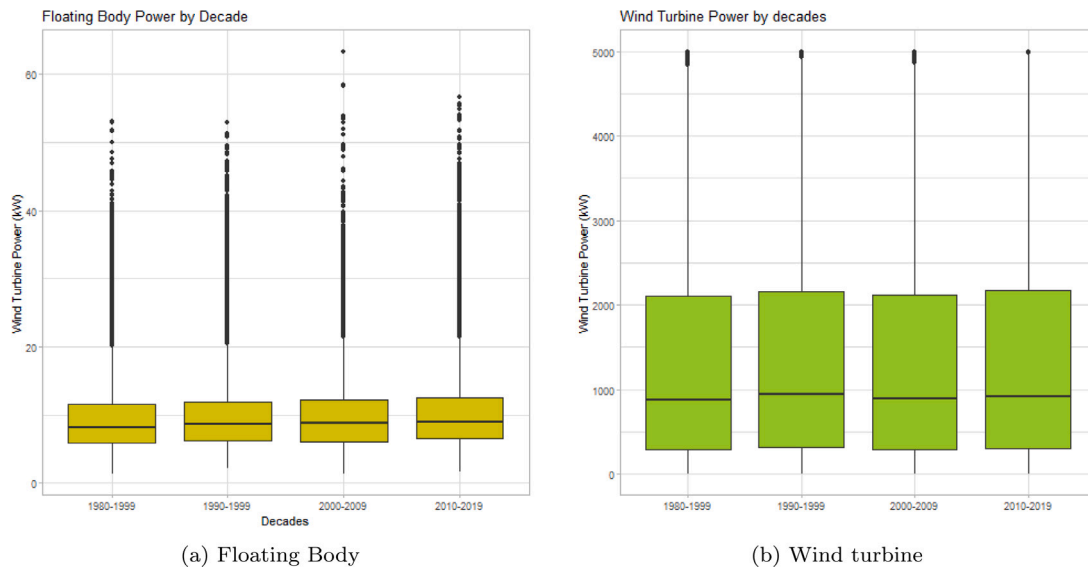
(a) Floating Body

(b) Wind turbine

Fig. 6. Power production in kW of the 5 MW wind turbine and the floating body WEC showing the boxplots corresponding to each decade. Each box shows the first and the third quartile in the up and down limits, and the median is represented by the line at the middle.
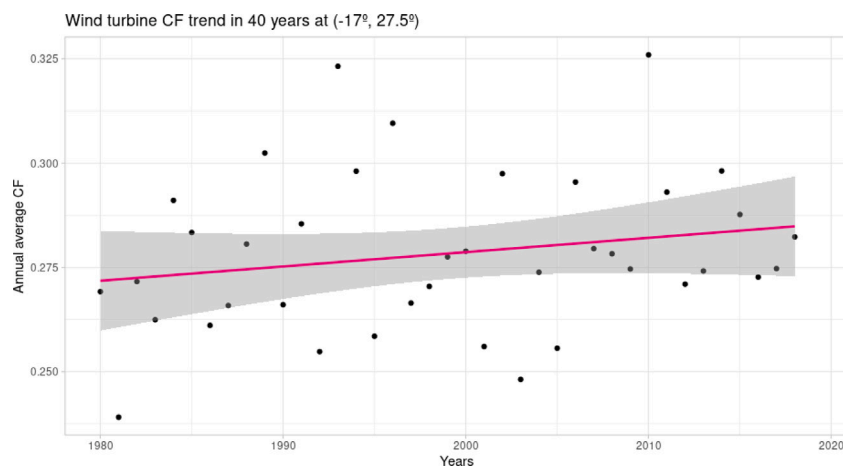

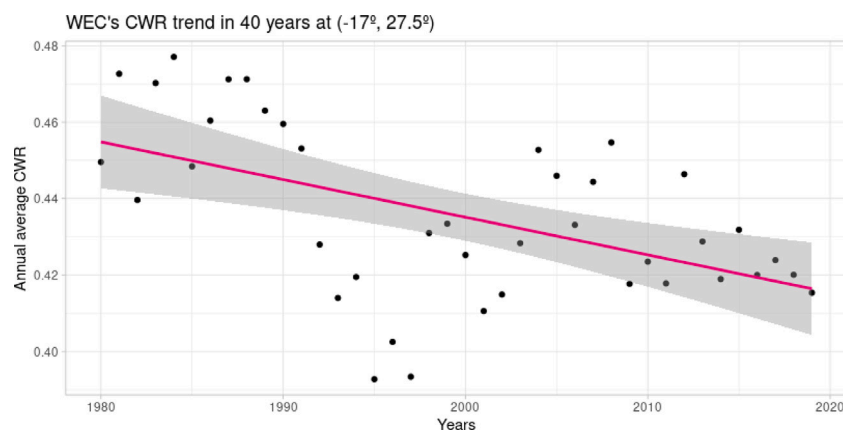**Fig. 7.** Capacity Factor trend at the identified hotspot of the selected wind turbine.

Fig. 8. Capture Width Ratio trend at the identified hotspot of the selected Wave Energy Converter.

already identified different physical causes that explain this expansion of the tropics, such as thermal forcing due to increased concentration of greenhouse gases, stratospheric ozone depletion anthropogenic aerosol forcing or even natural variability behind this expansion of the Hadley Cell [67]. These factors act differently at different seasons of the year, regions or hemispheres and this is still an area of open research. The last generations of climate models used in climate-change research have improved their ability to simulate the expansion of tropical belts [68]. In particular, results from these modelling exercises show that most part of the trend in the Northern Hemisphere is still inside the confidence interval due to natural variability as calculated from modelling results forced by preindustrial scenarios [69].

5. Conclusions

Canary Islands show great variations of available wind and wave energy during the last 40 years. This paper shows that hotspots can be identified due to these variations, where the co-location index for the feasibility of wind–wave energy combination is significantly affected above +5%/decade. The real variations of energy production for a given wind turbine and a given WEC during the study period also show an interesting decoupling that is related with the positive evolution of CLF. The corresponding CF trend for wind energy (+0.8%/decade) and CWR evolution for wave energy (−1.5%/decade) shows also the wind–wave decoupling for real electricity production. The authors did not find any other contribution in the scientific literature which shows such a significant decoupling of both oceanic energy sources in a multi-decadal time evolution, and even the idea of the study of long-term trend of wind–wave combination. Furthermore, the last results for real devices extend towards commercial aspects the previous results based on natural wind and wave energy flux.

Due to the location of the Canary Islands, under the influence of the trade winds, it can be identified a potential source of the variability isolated in this paper in changes of the Hadley Cell in the Atlantic basin, which have already been reported in other studies [70,71]. However, the effect pointed out here is quite local and ascribing this variability to global change-induced variability of the Hadley Cell or inter-annual variability of the Atlantic circulation is still an open problem which needs further study.

In other areas of the Atlantic, several positive trends mainly in wave energy flux have also been detected thus suggesting that they might be climate-driven [13,20]. However, more studies at the local level are needed to clearly relate climate oscillations and the observed wind and waves trends. Furthermore, various mathematical techniques such as Maximum Covariance Analysis can reinforce these kind of studies comparing the CLF technique described here with previous studies by the authors [16] or with other kind of multidimensional index proposals that incorporates the importance of extreme event with risk statistics. Techno-economic studies based on LCOE can help reducing subjectivity, and introducing more objective ratios between the selected weighs of an analogous CLF index.

Declaration of competing interest

The authors declare the following financial interests/personal relationships which may be considered as potential competing interests: Alain Ulazia reports financial support was provided by Spain Ministry of Science and Innovation.

Data availability

Data will be made available on request.

References

[1] Renewable Energy Statistics. Eurostat, EU. 2019, URL https://ec.europa.eu/eurostat/statistics-explained/index.php?title=Renewable_energy_statistics.

[2] Devezas T, LePoire D, Matias JC, Silva AM. Energy scenarios: Toward a new energy paradigm. Futures 2008;40(1):1–16.

[3] Potrč S, Čuček L, Martin M, Kravanja Z. Sustainable renewable energy supply networks optimization–The gradual transition to a renewable energy system within the European Union by 2050. Renew Sustain Energy Rev 2021;146:111186.

[4] Qiblawey Y, Alassi A, ul Abideen MZ, Bañales S. Techno-economic assessment of increasing the renewable energy supply in the Canary Islands: The case of Tenerife and Gran Canaria. Energy Policy 2022;162:112791.

[5] URL https://www.iea.org/policies/13323-climate-change-and-energy-transition-law.

[6] Ferrari F, Besio G, Cassola F, Mazzino A. Optimized wind and wave energy resource assessment and offshore exploitability in the Mediterranean sea. Energy 2020;190:116447.

[7] Wang W, Wu M, Palm J, Eskilsson C. Estimation of numerical uncertainty in computational fluid dynamics simulations of a passively controlled wave energy converter. Proc. Inst. Mech. Eng. M 2018;232(1):71–84.

[8] Uğurlu E. Renewable energy strategies for sustainable development in the European union. In: Renewable energy. Springer; 2019, p. 63–87.

[9] Héder M. From NASA to EU: The evolution of the TRL scale in public sector innovation. Innov. J. 2017;22(2):1–23.

[10] Ibarra-Berastegi G, Sáenz J, Ulazia A, Serras P, Esnaola G, Garcia-Soto C. Electricity production, capacity factor, and plant efficiency index at the Mutriku wave farm (2014–2016). Ocean Eng 2018;147:20–9.

[11] Villate J, Pirttimaa L, Cochrane C. Strategic research and innovation agenda for ocean energy. Tech. rep. 100513/BR/02, ETIP Ocean, Available at https://www.oceanenergy-europe.eu/wp-content/uploads/2020/05/ETIP-Ocean-SRIA.pdf. [Last accessed 14 Februrary 2023].

[12] Serras P, Ibarra-Berastegi G, Sáenz J, Ulazia A. Combining random forests and physics-based models to forecast the electricity generated by ocean waves: A case study of the Mutriku wave farm. Ocean Eng 2019;189:106314.

[13] Ibarra-Berastegi G, Ulazia A, Sáenz J, Serras P, Rojí SJG, Esnaola G, et al. The power flow and the wave energy flux at an operational wave farm: Findings from Mutriku, Bay of Biscay. Ocean Eng 2021;227:108654.

[14] Kulp SA, Strauss BH. New elevation data triple estimates of global vulnerability to sea-level rise and coastal flooding. Nature Commun 2019;10(1):1–12.

[15] Perez-Collazo C, Pemberton R, Greaves D, Iglesias G. Monopile-mounted wave energy converter for a hybrid wind-wave system. Energy Convers Manage 2019;199:111971.

[16] Saenz-Aguirre A, Saenz J, Ulazia A, Ibarra-Berastegui G. Optimal strategies of deployment of far offshore co-located wind-wave energy farms. Energy Convers Manage 2022;251:114914. http://dx.doi.org/10.1016/j.enconman.2021.114914.

[17] URL https://energy.ec.europa.eu/topics/energy-systems-integration/hydrogen_en.

[18] Carreno-Madinabeitia S, Ibarra-Berastegui G, Sáenz J, Ulazia A. Long-term changes in offshore wind power density and wind turbine capacity factor in the Iberian Peninsula (1900–2010). Energy 2021;226:120364. http://dx.doi.org/10.1016/j.energy.2021.120364.

[19] Ulazia A, Penalba M, Rabanal A, Ibarra-Berastegui G, Ringwood J, Sáenz J. Historical evolution of the wave resource and energy production off the Chilean coast over the 20th century. Energies 2018;11(9):2289. http://dx.doi.org/10.3390/en11092289.

[20] Ulazia A, Penalba M, Ibarra-Berastegui G, Ringwood J, Sáenz J. Reduction of the capture width of wave energy converters due to long-term seasonal wave energy trends. Renew Sustain Energy Rev 2019;113:109267. http://dx.doi.org/10.1016/j.rser.2019.109267.

[21] Penalba M, Ulazia A, Saénz J, Ringwood JV. Impact of long-term resource variations on wave energy farms: The Icelandic case. Energy 2020;192:116609.

[22] Latorre FJG, Quintana JJ, de la Nuez I. Technical and economic evaluation of the integration of a wind-hydro system in El Hierro island. Renew Energy 2019;134:186–93.

[23] Iglesias G, Carballo R. Wave resource in El Hierro—An island towards energy self-sufficiency. Renew Energy 2011;36(2):689–98.

[24] Veigas M, Iglesias G. Wave and offshore wind potential for the island of Tenerife. Energy Convers Manage 2013;76:738–45.

[25] Gonçalves M, Martinho P, Soares CG. Assessment of wave energy in the Canary Islands. Renew Energy 2014;68:774–84.

[26] Young I, Zieger S, Babanin AV. Global trends in wind speed and wave height. Science 2011;332(6028):451–5. http://dx.doi.org/10.1126/science.1197219.

[27] Megías E, García-Román M. Influence of trade winds on the detection of trans-hemispheric swells near the Canary Islands. Atmosphere 2022;13(4):505.

[28] Peña-Izquierdo J, Pelegrí JL, Pastor MV, Castellanos P, Emelianov M, Gasser M, et al. The continental slope current system between Cape Verde and the Canary Islands. Sci Mar 2012;76:65–78.

[29] Astariz S, Iglesias G. The collocation feasibility index–A method for selecting sites for co-located wave and wind farms. Renew Energy 2017;103:811–24.

[30] Aristondo O, Onaindia E. Decomposing energy poverty in three components. Energy 2023;263:125572.

[31] Hersbach H, Peubey C, Simmons A, Berrisford P, Poli P, Dee D. ERA-20CM: a twentieth-century atmospheric model ensemble. Q J R Meteorol Soc 2015;141(691):2350–75. http://dx.doi.org/10.1002/qj.2528.

[32] Peuch V-H, Engelen R, Rixen M, Dee D, Flemming J, Suttie M, et al. The copernicus atmosphere monitoring service: From research to operations. Bull Am Meteorol Soc 2022;103(12):E2650–68.

[33] Olauson J. ERA5: The new champion of wind power modelling? Renew Energy 2018;126:322–31. http://dx.doi.org/10.1016/j.renene.2018.03.056.

[34] Ulazia A, Esnaola G, Serras P, Penalba M. On the impact of long-term wave trends on the geometry optimisation of oscillating water column wave energy converters. Energy 2020;206:118146. http://dx.doi.org/10.1016/j.energy.2020.118146.

[35] Bruno MF, Molfetta MG, Totaro V, Mossa M. Performance assessment of ERA5 wave data in a swell dominated region. J Mar Sci Eng 2020;8(3):214. http://dx.doi.org/10.3390/jmse8030214.

[36] Rusu L, Rusu E. Evaluation of the worldwide wave energy distribution based on ERA5 data and altimeter measurements. Energies 2021;14(2):394. http://dx.doi.org/10.3390/en14020394.

[37] Shi H, Cao X, Li Q, Li D, Sun J, You Z, et al. Evaluating the accuracy of ERA5 wave reanalysis in the water around China. J Ocean Univ China 2021;20(1):1–9. http://dx.doi.org/10.1007/s11802-021-4496-7.

[38] Font-Tullot I. Climatología de España y Portugal. 2nd ed. Ed. Universidad de Salamanca; 2000, p. 422.

[39] Iqbal MJ, Rehman SU, Hameed S, Qureshi MA. Changes in Hadley circulation: the Azores high and winter precipitation over tropical northeast Africa. Theor Appl Climatol 2019;137:2941–8. http://dx.doi.org/10.1007/s00704-019-02765-4.

[40] Ramos-Real FJ, Barrera-Santana J, Ramírez-Díaz A, Perez Y. Interconnecting isolated electrical systems. The case of Canary Islands. Energy Strategy Rev 2018;22:37–46.

[41] EMODnet Bathymetry Consortium. EMODnet digital bathymetry (DTM). 2020, http://dx.doi.org/10.12770/bb6a87dd-e579-4036-abe1-e649cea9881a.

[42] Bidlot J. Ocean wave model output parameters. 2020, URL https://confluence.ecmwf.int/display/CKB/ECMWF+Model+Documentation?preview=/59774192/59774191/wave_parameters.pdf.

[43] Multon B. Marine renewable energy handbook. John Wiley & Sons; 2013.

[44] Details Parameters. ECMWF. 2022, Online https://apps.ecmwf.int/codes/grib/param-db/?id=140112. [Accessed 5 November 2022].

[45] Sáenz J, González-Rojí SJ, Carreno-Madinabeitia S, Ibarra-Berastegi G. Analysis of atmospheric thermodynamics using the R package aiRthermo. Comput Geosci 2019;122:113–9.

[46] Sáenz J, González-Rojí SJ, Carreno-Madinabeitia S, Ibarra-Berastegi G. aiRthermo: Atmospheric thermodynamics and visualization. 2018, R package version 1.2.1 URL https://CRAN.R-project.org/package=aiRthermo.

[47] Ulazia A, Sáenz J, Ibarra-Berastegi G, González-Rojí SJ, Carreno-Madinabeitia S. Global estimations of wind energy potential considering seasonal air density changes. Energy 2019;187:115938. http://dx.doi.org/10.1016/j.energy.2019.115938.

[48] Ulazia A, Ibarra-Berastegi G, Sáenz J, Carreno-Madinabeitia S, González-Rojí SJ. Seasonal correction of offshore wind energy potential due to air density: Case of the Iberian Peninsula. Sustainability 2019;11(13):3648.

[49] Theil H. A rank-invariant method of linear and polynomial regression analysis, 3; confidence regions for the parameters of polynomial regression equations. Stickst Math Cent Stat Afdeling 1950;1–16.

[50] Jonkman J, Butterfield S, Musial W, Scott G. Definition of a 5-MW reference wind turbine for offshore system development. Tech. rep., Golden, CO (United States): National Renewable Energy Lab.(NREL); 2009.

[51] Manwell JF, McGowan JG, Rogers AL. Wind energy explained: Theory, design and application. John Wiley & Sons; 2010.

[52] Oigarden H, Olsen F. Wave power station. 2009, US Patent US7585131B2 URL https://patents.google.com/patent/US7585131B2/en.

[53] Khan M, Khalid A, Lughmani WA, Khan MM. A use case of exclusive economic zone of Pakistan for wave power potential estimation. Ocean Eng 2021;237:109664. http://dx.doi.org/10.1016/j.oceaneng.2021.109664.

[54] Mederos AM, Padrón JM, Lorenzo AF. An offshore wind atlas for the canary islands. Renew Sustain Energy Rev 2011;15(1):612–20.

[55] Bosch J, Staffell I, Hawkes AD. Temporally explicit and spatially resolved global offshore wind energy potentials. Energy 2018;163:766–81.

[56] Babarit A. A database of capture width ratio of wave energy converters. Renew Energy 2015;80:610–28. http://dx.doi.org/10.1016/j.renene.2015.02.049.

[57] Zheng CW, Wang Q, Li CY. An overview of medium- to long-term predictions of global wave energy resources. Renew Sustain Energy Rev 2017;79:1492–502. http://dx.doi.org/10.1016/j.rser.2017.05.109.

[58] TUoD DTU. Global wind atlas 3.0. Denmark: Vortex Lyngby; 2022, Online https://globalwindatlas.info/. [Accessed 5 November 2022].

[59] Aristondo O, Onaindia E. Inequality of energy poverty between groups in Spain. Energy 2018;153:431–42.

[60] Martinez A, Iglesias G. Mapping of the levelised cost of energy for floating offshore wind in the European Atlantic. Renew Sustain Energy Rev 2022;154:111889.

[61] Chang G, Jones CA, Roberts JD, Neary VS. A comprehensive evaluation of factors affecting the levelized cost of wave energy conversion projects. Renew Energy 2018;127:344–54.

[62] Astariz S, Perez-Collazo C, Abanades J, Iglesias G. Co-located wind-wave farm synergies (Operation & Maintenance): A case study. Energy Convers Manage 2015;91:63–75.

[63] Decancq K, Lugo MA. Weights in multidimensional indices of wellbeing: An overview. Econometric Rev 2013;32(1):7–34.

[64] Marrero-Betancourt N, Marcello J, Rodríguez-Esparragón D, Hernández-León S. Wind variability in the Canary current during the last 70 years. Ocean Sci 2020;16:951–63. http://dx.doi.org/10.5194/os-16-951-2020.

[65] Hu Y, Huang H, Zhou C. Widening and weakening of the Hadley circulation under global warming. Sci Bull 2018;(63):640–4. http://dx.doi.org/10.1016/j.scib.2018.04.020.

[66] Grise KM, Davis SM, Staten PW, Adam O. Regional and seasonal characteristics of the recent expansion of the tropics. J Clim 2018;31:6839–56. http://dx.doi.org/10.1175/JCLI-D-18-0060.1.

[67] Grise KM, Davis SM, Simpson IR, Waugh DW, Fu Q, Allen RJ, et al. Recent tropical expansion: Natural variability or forced response? J Clim 2019;32:1551–71. http://dx.doi.org/10.1175/JCLI-D-18-04444.1.

[68] Grise KM, Davis SM. Hadley cell expansion in CMIP6 models. Atmos Chem Phys 2020;20:5249–68. http://dx.doi.org/10.5194/acp-20-5249-2020.

[69] Staten PW, Grise KM, Davis SM, Karnaukas KB, Waugh DW, Maycock AC, et al. Bull Am Meteorol Soc 2020;101:E897–904. http://dx.doi.org/10.1175/BAMS-D-19-0047.1.

[70] Kang SM, Lu J. Expansion of the Hadley cell under global warming: Winter versus summer. J Clim 2012;25(24):8387–93.

[71] Lau WK, Kim K-M. Robust hadley circulation changes and increasing global dryness due to CO2 warming from CMIP5 model projections. Proc Natl Acad Sci 2015;112(12):3630–5.